

In-situ

K. C. Wang, L. H. Cheng, L. Essler, G. T. Pollock

Gemological Institute, China University of Geosciences, Wuhan 430074, PR China
 Hubei Gem and Jewelry Engineering Technology Research Center, Wuhan 430074, PR China
 School of Materials Science and Engineering, Huazhong University of Science and Technology, Wuhan 430074, PR China
 Mechanical Engineering, University of Birmingham, Birmingham B15 2TT, UK
 School of Electrical and Electronic Engineering, Huazhong University of Science and Technology, Wuhan 430074, PR China
[†]WMG, Materials Engineering Centre, University of Warwick, CV4 7AL Coventry, UK

ARTICLE INFO

Keywords:

Titanium matrix composites
 Carbon fiber
 SLM
 CVD
 EMI

ABSTRACT

Carbon fiber reinforced titanium matrix composites (3DG) fabricated by selective laser melting (SLM) and chemical vapor deposition (CVD). The composites were characterized by scanning electron microscopy (SEM), energy-dispersive X-ray (EDS), and X-ray diffraction (XRD). The tensile properties of the composites were investigated. The results show that the composites have a high tensile strength and modulus. The CVD process significantly improved the interfacial bonding between the carbon fibers and the titanium matrix. The EMI shielding effectiveness (SE) of the composites was also evaluated. The SE of the composites was significantly improved by the CVD process. The SE of the composites was 47.8 dB at 2.7 GHz and 32.3 dB at 18 GHz. The results indicate that the CVD process is an effective method for improving the properties of carbon fiber reinforced titanium matrix composites.

1. Introduction

Carbon fiber reinforced titanium matrix composites (C/TMCs) have attracted significant attention due to their high strength-to-weight ratio and excellent mechanical properties. However, the poor interfacial bonding between carbon fibers and titanium matrix is a major challenge for the development of C/TMCs. Chemical vapor deposition (CVD) is a promising method for improving the interfacial bonding between carbon fibers and titanium matrix. In this study, carbon fiber reinforced titanium matrix composites (3DG) were fabricated by selective laser melting (SLM) and CVD. The composites were characterized by scanning electron microscopy (SEM), energy-dispersive X-ray (EDS), and X-ray diffraction (XRD). The tensile properties of the composites were investigated. The results show that the composites have a high tensile strength and modulus. The CVD process significantly improved the interfacial bonding between the carbon fibers and the titanium matrix. The EMI shielding effectiveness (SE) of the composites was also evaluated. The SE of the composites was significantly improved by the CVD process. The SE of the composites was 47.8 dB at 2.7 GHz and 32.3 dB at 18 GHz. The results indicate that the CVD process is an effective method for improving the properties of carbon fiber reinforced titanium matrix composites.

*Corresponding author. E-mail address: wangkc@cug.edu.cn (K.C. Wang).

l s . T X s s s (. . , s -
s) , X fl fi l s -
(. . , l ss, f s) f 3DG. B s s, -
3DG ll s f l l
(. . , s , s , s f l). H , s f s
l l s l s ffi l
s l l s , f s , l N f
ll s s l ll f
, s s l 3DG s s l f -
s s s f s f s fi f l s 17,18 .
H , s f ss l l l s,
s l l f s s 3DG
l s s s l f s 19 .
S l l s l (SLM), s -
f (AM) l , s l l s f f
f s s / s X - s l (3D) l l s
s f l X s , ffi
fi X l f in-situ f l . T , s
s s SLM s s s f T ll s 20 ,
s l ss ll s 21 , N ll s 22 . C s s l s f l /
s s f l - s s s - f - -
s s l s . C N s s ,
s s s l s s f
CVD l s l (< 0.001 .%)
ss s l f , -
l s l l l s 23 . W l N s
s l l (> 0.1 .%) 17 , fi s
f s f X ss 24 . H , -
s SLM f s s ll s f s ffi
f s l f s s l
fl s l s l
(1000-1100) . F f s s s ff l s
SLM s s ll f ll s 25 .
T l s , f fi s s
f s l - 3DG/ (3DG/C) s -
s SLM s l s CVD f
. A ll- s s l l s
ll s SLM f s l l -

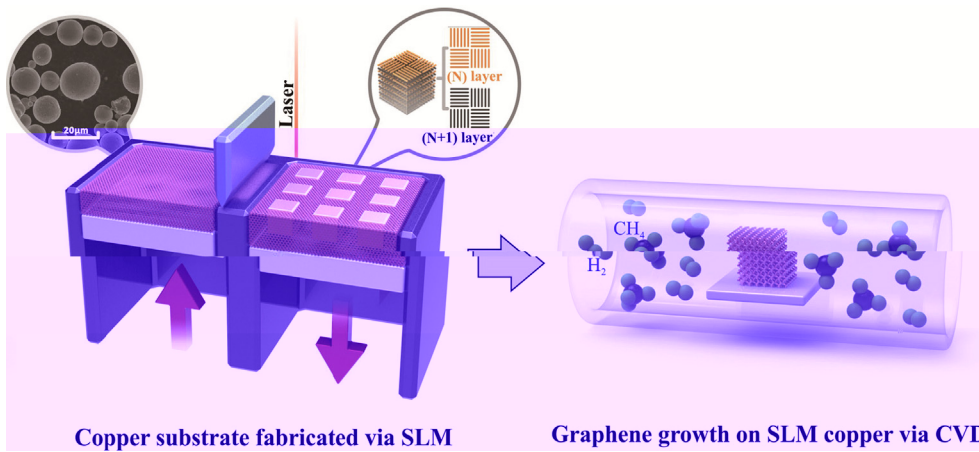


Fig. 1. Schematic diagram of the SLM process for copper substrate fabrication and subsequent in-situ CVD for graphene growth.

ASTM B193-2002 (5) (2) (3) (4) (5) (6) (7) (8) (9) (10) (11) (12) (13) (14) (15) (16) (17) (18) (19) (20) (21) (22) (23) (24) (25) (26) (27) (28) (29) (30) (31) (32) (33) (34) (35) (36) (37) (38) (39) (40) (41) (42) (43) (44) (45) (46) (47) (48) (49) (50) (51) (52) (53) (54) (55) (56) (57) (58) (59) (60) (61) (62) (63) (64) (65) (66) (67) (68) (69) (70) (71) (72) (73) (74) (75) (76) (77) (78) (79) (80) (81) (82) (83) (84) (85) (86) (87) (88) (89) (90) (91) (92) (93) (94) (95) (96) (97) (98) (99) (100)

3. Results and discussion

3.1. Formation of SLM copper

3.1.1. SLM manufacturing of copper under different line energy densities

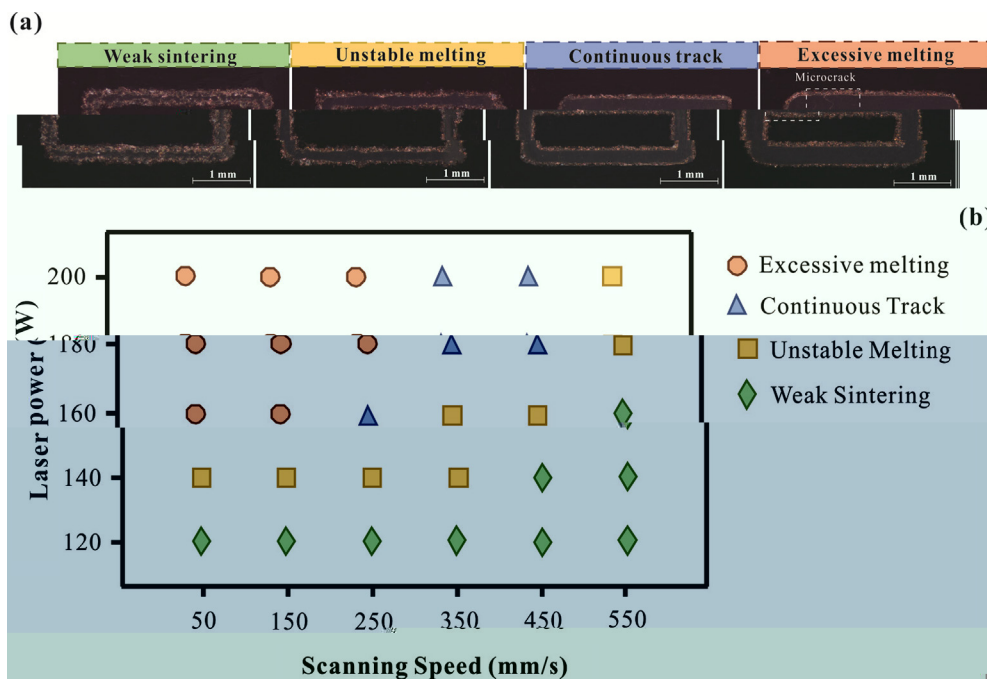


Fig. 2. (a) SEM images of SLM copper tracks under different conditions. (b) Scatter plot of Laser power (W) vs Scanning Speed (mm/s) for different conditions.

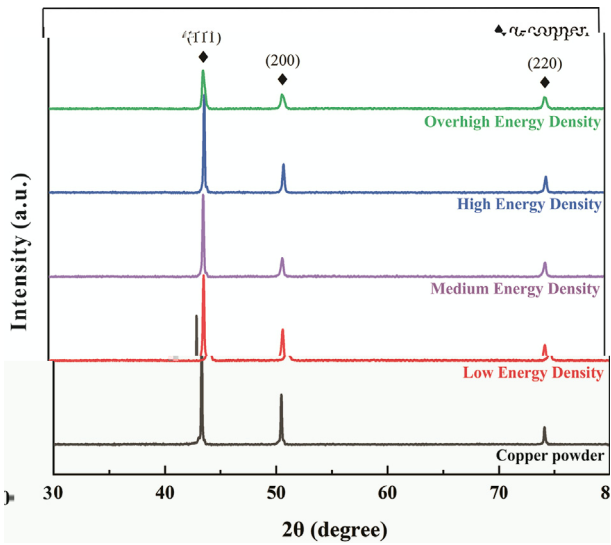


Fig. 3. RD patterns of copper powder at different energy densities.

3.1.2. Formation of anisotropic microstructure under different volumetric energy density

The XRD patterns of copper powder at different energy densities are shown in Fig. 3. The intensity of the (111) peak is significantly higher than that of the (200) and (220) peaks at 43.32°, 50.45°, and 58.63° 2θ, respectively. This indicates that the copper powder has a strong preferred orientation along the (111) plane. The preferred orientation of copper powder is further confirmed by the pole figure (PF) plot in Fig. 4. The PF plot shows that the (111) plane is the most preferred orientation, with a maximum intensity of 3.1. The intensity of the (111) plane is significantly higher than that of the (200) and (220) planes. This indicates that the copper powder has a strong preferred orientation along the (111) plane. The preferred orientation of copper powder is further confirmed by the pole figure (PF) plot in Fig. 4. The PF plot shows that the (111) plane is the most preferred orientation, with a maximum intensity of 3.1. The intensity of the (111) plane is significantly higher than that of the (200) and (220) planes. This indicates that the copper powder has a strong preferred orientation along the (111) plane.

The XRD patterns of copper powder at different energy densities are shown in Fig. 3. The intensity of the (111) peak is significantly higher than that of the (200) and (220) peaks at 43.32°, 50.45°, and 58.63° 2θ, respectively. This indicates that the copper powder has a strong preferred orientation along the (111) plane. The preferred orientation of copper powder is further confirmed by the pole figure (PF) plot in Fig. 4. The PF plot shows that the (111) plane is the most preferred orientation, with a maximum intensity of 3.1. The intensity of the (111) plane is significantly higher than that of the (200) and (220) planes. This indicates that the copper powder has a strong preferred orientation along the (111) plane. The preferred orientation of copper powder is further confirmed by the pole figure (PF) plot in Fig. 4. The PF plot shows that the (111) plane is the most preferred orientation, with a maximum intensity of 3.1. The intensity of the (111) plane is significantly higher than that of the (200) and (220) planes. This indicates that the copper powder has a strong preferred orientation along the (111) plane.

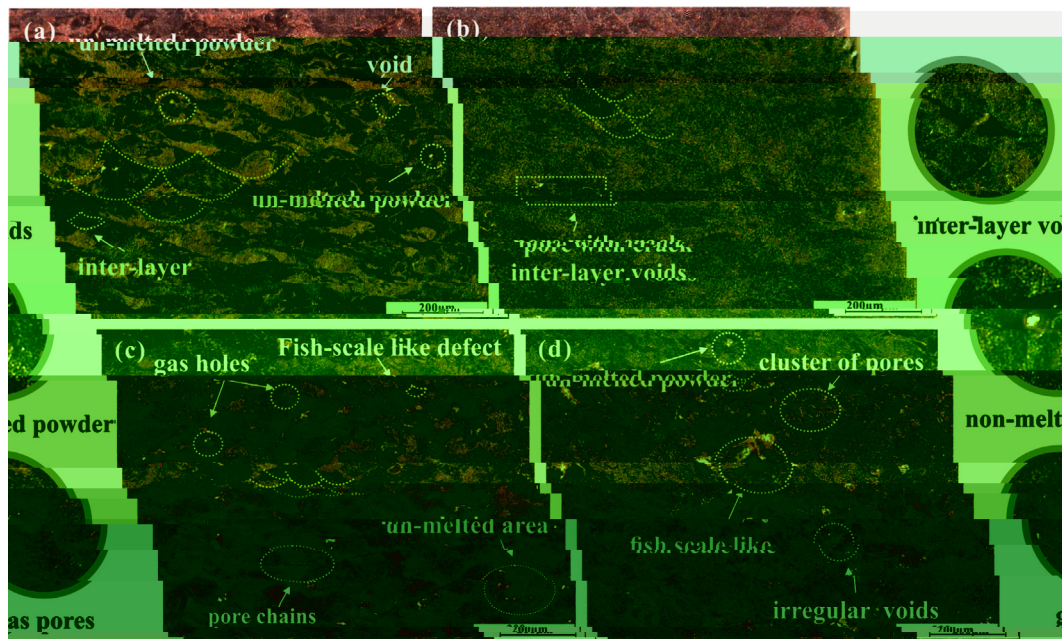


Fig. 4. SEM micrographs of SLM-processed copper powder at different energy densities: (a) 285 J/cm³, (b) 128 J/cm³, (c) 3000 J/cm³, (d) 857 J/cm³.

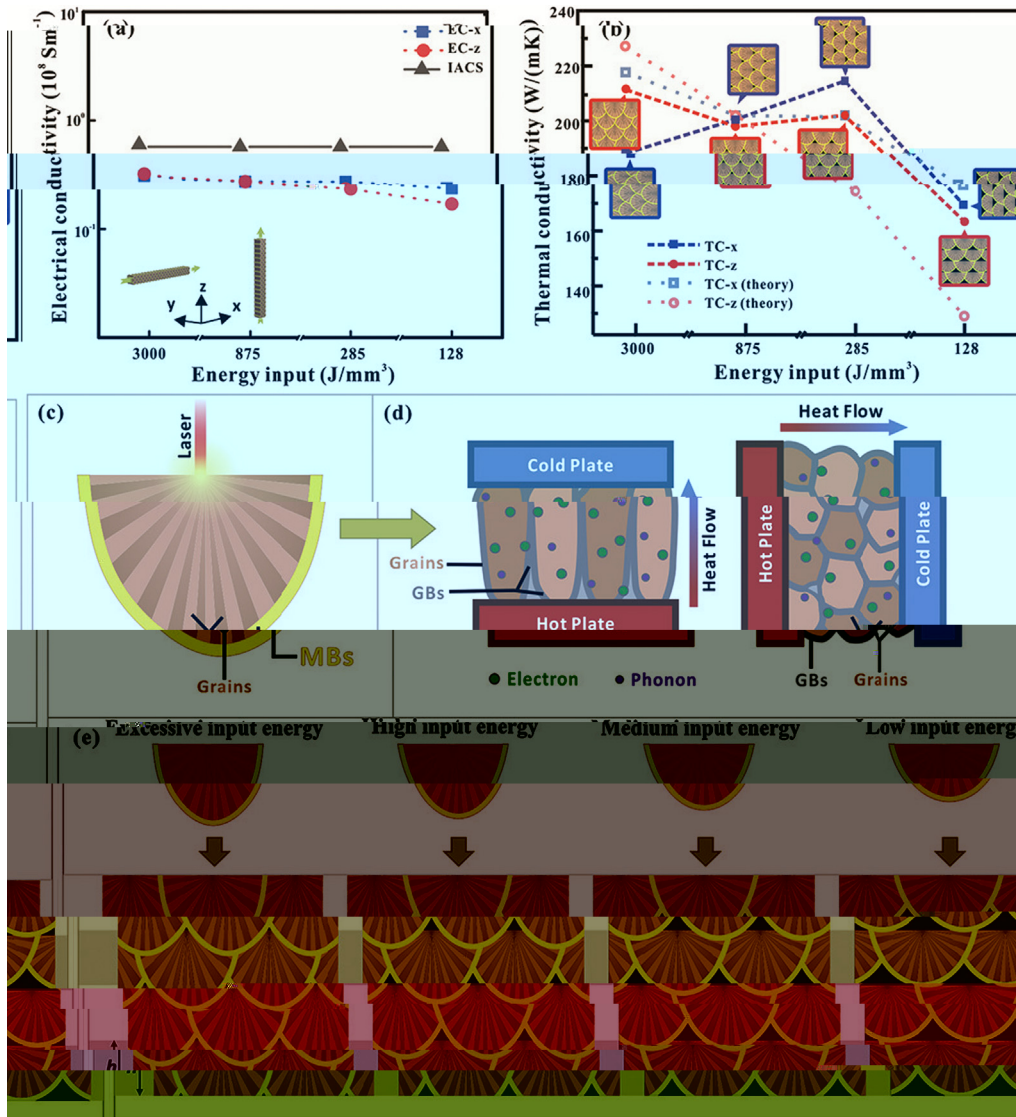


Fig. 7. (a) Electrical conductivity vs. energy input for TC-x, EC-z, and IACS. (b) Thermal conductivity vs. energy input for TC-x, TC-z, and their theoretical values. (c) Schematic of laser irradiation on a porous scaffold. (d) Schematic of heat flow through a porous scaffold between hot and cold plates. (e) Schematic showing the effect of different energy input levels on the porous scaffold structure.

SEM, 3DGC/C, 450 μm (F . 8a). A SEM (F . 8b), EDS (F . 8c-d), (F . 8e-g). T 3DGC/C (F . 8h). 3DGC/C (~1590 m^{-1}) s 2D- (~2699 m^{-1}) s G- (~1350 m^{-1}) fl s 42 (F . 8). S 43, (D G s (I_D/I_G) s

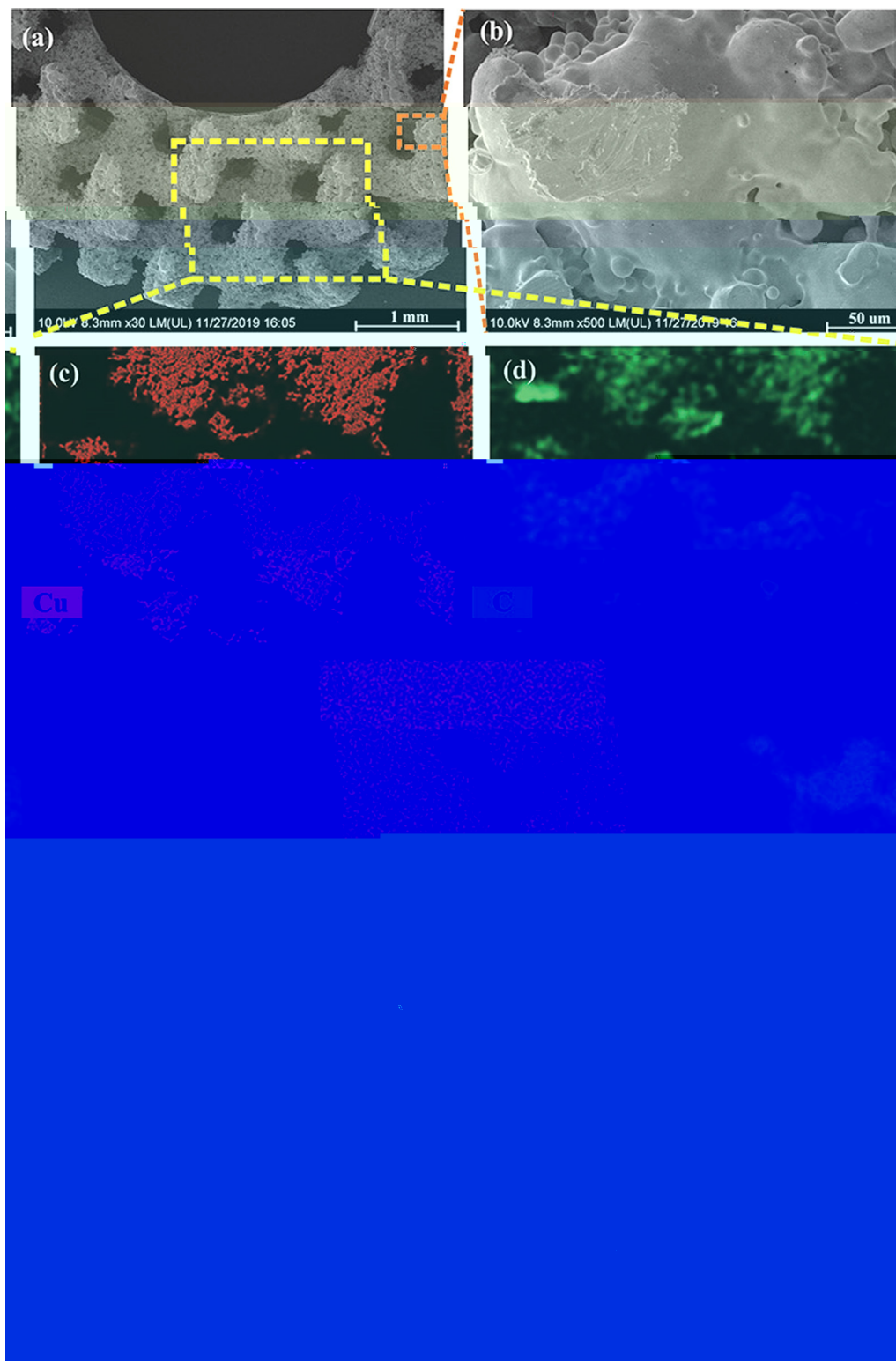


Fig. 8. (a) SEM image of 3DG/Cu porous scaffold at 30x magnification. (b) SEM image of 3DG/Cu porous scaffold at 500x magnification. (c) EDS elemental map for Copper (Cu). (d) EDS elemental map for Carbon (C).

3.4. Thermal property and EMI shielding effectiveness of 3DG/Cu porous scaffolds

The thermal stability of the 3DG/Cu porous scaffolds was evaluated by TGA. The TGA curves of 3DG/Cu porous scaffolds with different Cu contents (0, 10, 20, 30, 40, 50, 60, 70, 80, 90, 100 wt%) are shown in Fig. 9. The TGA curves show that the 3DG/Cu porous scaffolds exhibit good thermal stability. The weight loss of the 3DG/Cu porous scaffolds is mainly due to the decomposition of the 3DG component. The weight loss of the 3DG/Cu porous scaffolds increases with the increase of the Cu content. The weight loss of the 3DG/Cu porous scaffolds is 26.8% at 1000 °C for the 3DG/Cu porous scaffold with 0 wt% Cu, and 14.8% for the 3DG/Cu porous scaffold with 100 wt% Cu.

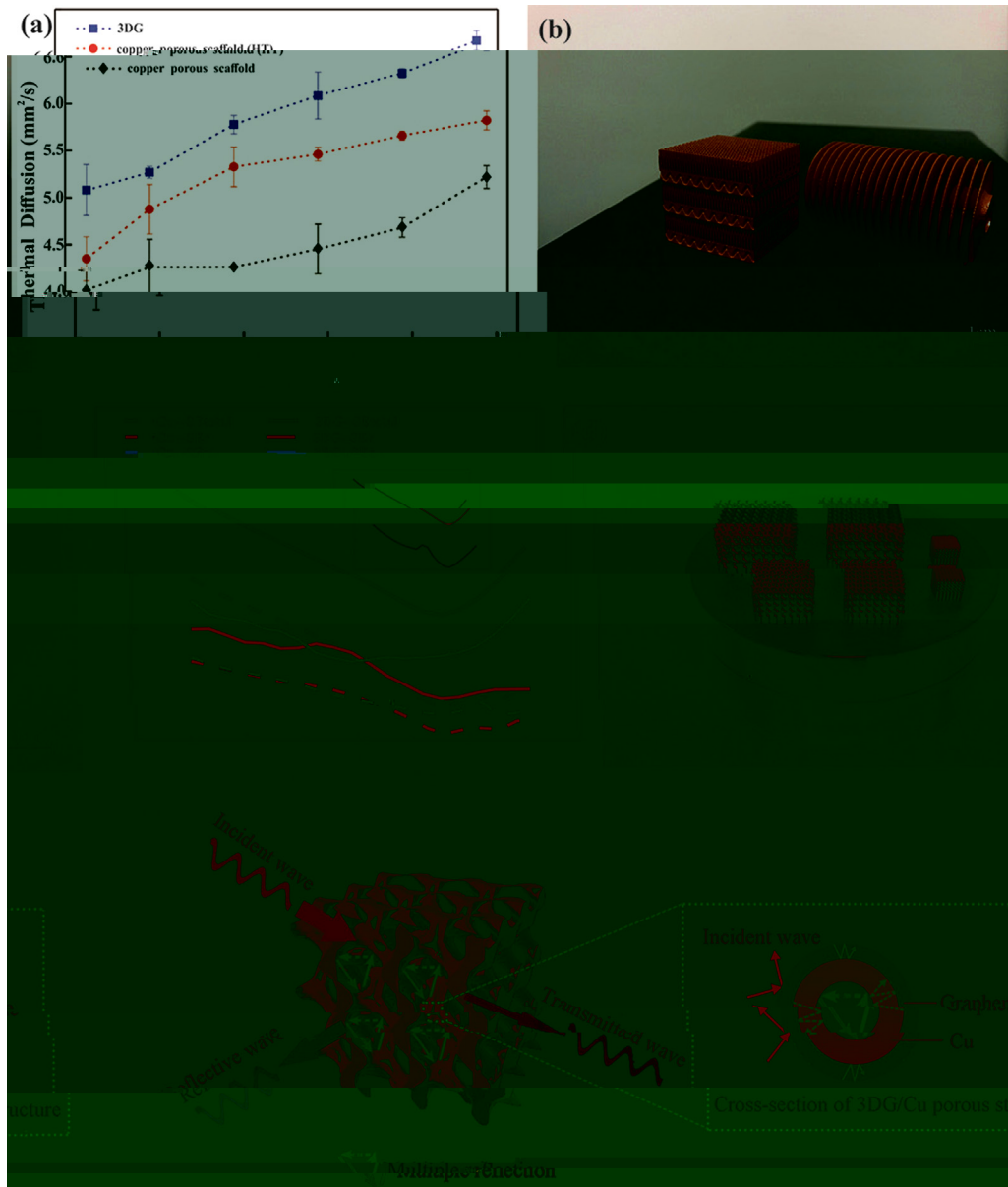


Fig. 9. Thermal Diffusion (mm²/s) vs. Temperature (°C) for 3DG/Cu porous scaffold (3DG/Cu porous scaffold, 3DG/Cu porous scaffold). (a) Thermal Diffusion (mm²/s) vs. Temperature (°C) for 3DG/Cu porous scaffold (3DG/Cu porous scaffold, 3DG/Cu porous scaffold). (b) 3D model of a porous scaffold structure.

Table 1

Coating materials	Substrate	Method	Maximum shielding efficiency (dB)	Improvement of thermal property (%)	Ref
G	G	SLM	37	-	50
G	PS	SLM	29.3	-	56
G	PMMA	SLM	19	-	57
C /G	/C	SLM	-	8.5	58
G	N	CVD	-	554	59
G	C -N	SLM	20	-	60
G	C	SLM + CVD	-	2.4	61
G	3DG/C	SLM	47	6.3	62
G	C	CVD + SLM	47.8	27	62

Note: () -PPMA, () -PS.

HT s ↓ s s s s
in-situ (F . 9a). S s ↓ - - ↓ s -
 f s f 3DG/C s s ff ↓ ss ss s -
 . I s ↓s HT s ↓ ↓s
 1-2 s f . I s s , s s
 f s s sf . W
 s ↓ ssfl X (, s s SLM s
 ↓ ss 500 μ) ↓ - s s s sff ↓
 f X (F . 9b), f s s ↓ f ↓
 s -s . G ↓ s ↓ s -
 ↓s s s, s f s ↓ , f ss,
 f s ↓
 f f f ↓ s s
 (T ↓ 1). I ↓ s s X s f ↓
 s ↓ s ↓ s s. O ↓ -
 s , ↓ N ↓ . ↓ ↓ ↓
 T s ↓ f 3DG/C s s ff ↓ f
 EMI, EMI SE, s s ↓
 ↓ (EM) s s f
 f 2-18 GH (F . 9c), X s ↓ f
 f . W *in-situ*
 s s ff ↓ , SE s f 15.9 32.3 B,
 ↓ f 47.8 B (88.2% s), f s ss -
 ↓ ↓ f ↓ f 20 B. T ↓ ↓
 ↓ s f 3DG/C fi f
 s s . J K ↓ . 44 EMI f
 s s s s . T EMI SE
 s (. , s ↓ s) f 20 110 PPI (s s).
 R J* K s 45 ↓ s s
 s f f EMI
 f . W f s ↓ s ↓ s s s
 f 17 26 PPI (F . 9c insert) 105%
 EMI SE. I s, EMI s ↓ s J*s
 s ff ↓ s f ↓ s f SLM. T
 3DG/C s s 26 PPI X EMI SE f
 32.3 B, s 99.9% ↓ f EMI s. T s
 ↓ ↓ f s ↓ f s s ff ↓) 46 . T EMI
 s ↓ f s f 3DG/C s ↓ - s -
 ↓s ↓s ↓s T ↓ s 1. I ↓ EMI SE f
 3DG/C s s ↓ s f
 ↓ 3D - s s, ↓ ↓ s
 ↓ ↓ s s f EMI s s f fl (SE_r), s
 (SE_a) ↓ ↓ fl s f ↓ (EM) s 47 ,
 ↓ ↓ s, f s f s ↓ ↓s, s ↓
 48 . R s s 49 f ↓ ↓
 ↓ ↓ s , ↓ ↓ s ↓ fl ↓
 s, s X s s f ↓ s ↓ s.
 T s s EM
 ↓ ss s ↓ f s ↓ fi ↓
 ↓ s ↓ s 50 . R s s EMI X ↓
 s . T s ↓ s s f - X -
 s ↓ fl ↓ s, s s C 51 . F f
 s - X s ↓ f s -
 ↓ S O₂ 52 53 . W f s
 3DG/C s s ff ↓ s s f

s s s ↓ s s s fi s f
 SE_r SE_a, s s ↓ s s F . 9e. W s
 s f f 3DG/C s s ff ↓ , s
 ↓ fl s s ff ↓ . S ↓ -
 s ↓ s f 3DG/C s s -
 s f f s f fl s s s f
 s ↓ s. T
 EM s fi s ↓ ↓
 s ↓ s EM s, s ↓
 f ↓ ss f SE_r, O
 , s ff ↓ , s ↓ fi ↓ EM
 s ff ↓ , s s ↓, EM -
 s ss s s s. T
 f s ↓ ff s ↓
 J ↓ 54 . I s
 fl ↓ ↓ s
 ↓ ↓ ↓ f f fl ff s. M ,
 ↓ s f s f
 ↓ ↓ s s , f ↓ ↓ s f s
 s f s, f ↓ ↓ fl s s f
 EM s s ↓ s f ss f
 EM s. T s f s ↓
 s f 44 . T s s ss s
 ↓ s 3D s ↓ ↓
 ↓ s s X s f CVD f s s
 ↓ s s R s s f f s -
 s s s ↓ S 3.3 ↓ s s s X s
 ↓ ss s s ↓ ↓
 s ↓ f 55 . I s ↓
 EM s ↓ f s s, s
 s f ↓ ↓ ss. O ↓ ,
 s s f 3DG/C s s
 fl , s , s fl
 s ↓ . T ↓ ↓ ss
 s f s ff ↓ f s
 sf .

4. Conclusions

A ↓ 3DG/C s s ff ↓ s s ssf ↓ f
 s ↓ *in-situ* s f ↓ CVD .
 T s s s s
 f s s ff ↓ f . W
 s s ↓ f s s , 3DG/C
 s s ↓ EMI SE f
 15.9 (f f s ↓) 32.3 B, X
 f 47.8 B (88.2% s), s ↓ s 26.8% s ↓
 ff s . T 3DG/C s ↓ s
 ff s fl , s ↓ ↓ fl s ↓ -
 s s. T s J*s s EMI ↓
 3DG/C s s ff ↓ s s ↓ f
 ↓ s EMI s ↓ ↓ .

Credit authorship contribution statement

Kaka Cheng: C ↓ , M ↓ , F ↓ ↓ s s,
 W - ↓ f . Wei Xiong: V ↓ , I s , W -
 ↓ f . Yan Li: W - & , F s ,
 R s s, S s . Liang Hao: F s . Chunze Yan:
 R s s, F s . Zhaoqing Li: V ↓ . Zhufeng Liu:
 F ↓ ↓ s s. Yushen Wang: I s , S f . Khamis Essa:
 W - & . Li Lee: D . Xin Gong: S f .
 Ton Peijs: W - & , S s .

Declaration of Competing Interest

T s l s fl f s
l f s .

Acknowledgement

T s f ll l fi l s f
N l N l S F f C (N . 51671091, N .
51902295, N . 51675496). T
F l R s F s f C l U s s, C
U s f G s s (W) (N . (N . CUG170677) H
P N l S F (N . 2019 CFB264).

Appendix A. Supplementary data

S l s l f l s://
. /10.1016/ s s .2020.105904.

References

1 B RG, N N, M s K, M S. G : s l l f f
s s ss .P M S 2018;91:24-69.
2 B l AA, G s S, B W, C l, T l D, M F, l S
f s l l N L 2008;8(3):902-7.
3 L , H, C s M, P l H, P O, S l G, l I s X -
f l f s s f l s f f i l s l
s s. ACS A l M I f s 2016;8(36):24112-22.
4 K M, K J, J B, C , K JH, A JH. G - s - s l
s s f l l s. ACS N 2017;11(8):7950-7.
5 P , C M, H M, T M, , L D. P
s l f f - s l l l l
A l C l B 2020;262:118266-76.
6 L J, W, C LL, J SH, W G, L, l F l C-G f
l s s l .C s P A
2017;101:50-8.
7 HQ, L SW, C LH, J SH, H HQ. S l f -
- f l - s. J M C A
2018;6(42):21216-24.
8 D l s TM, S P, D s P, K J, K M, A s T, l 3D -
- s- l l l l l l s f s l s
l l l s f H . P C . P s 2017;1(4):467-70.
9 Q L, L L. T s l s l s s f l s s f l s X s .
ss l f l s f l s s f l s X s .
RSC A 2014;4(72):38273-80.
10 D , H L SP, N, W X JG. 3D X -
M S2 : P s l s -
f . C s P A 2016;90:424-32.
11 L L, W, S CO, H MK, HL, D W, l S l f ss l -s ll
- f ll s s s 3D f l s fi EM -
s f . A F M 2018. s:// . /10.1002/ f .
201803938.
12 L J, P , C, R G, , N l s D, l G
s S O2 s s f l s s. ACS N
2013;7(7):6001-6.
13 J SH, A l S, G A. L - s ll l s s s f l
l s. A C I E 2017;56:15520-38.
14 I , T , S K, K s M, T s T, T K, l. T -
s l s s l - s l
s. PCCP 2018;20(9):6024-33.
15 S K, D N, M ll C, V s l N, E l J. T ll l
l J E l S 2002;149(8):370-7.
16 C H, S M, S WH, L G, H , Q, l P f l 3D
l s f s s s ll 2011;7(22):3163-8.
17 K s H, G X M, J s l, H J, W C, C M. U
f s l f f - s l - s l
. M 2019;1(4):1077-87.
18 S Q, F , L W, L H, L , l C - l l
- s ll l f s f l - f - l l
f l s l . A M 2017;29(31):1701583-90.
19 , G C, L, T H, D, W , l. T s ll f -
f l f s s f
s. ACS N 2019. s:// . /10.1021/ s .9 08191.
20 C C, H , B , N J, C S, L F, l 3D s T 6A l 4V :
ff s f l s f l s l ;
l l M D s 2019;175:107824-33.
21 S š č J, B ž č D. T ff f NB s f l -
s f 316L s ll s s l s l s SLM. S f C
T l 2016;307:407-17.

22 R DC, HB, L J, L SJ, J W, R, l M s
f T-N ll f s l l s l . M S E A-S
2020;771:138586-95.
23 L , C W, A J, K S, N J, D, l L - s s s f - l
f f l s f l s. S 2009;324(5932):1312-4.
24 C P, R WC, G LB, L BL, P SE, C HM. T - s l f l l
s . N M 2011;10:424-8.
25 J SD, D s S, G ss s L, K JP, H X JV, V s l K.
I fl f s l l s l ss s X l
. J M P ss T l 2019;270:47-58.
26 W, H L, L , T D, C Q, F , l. Eff (s l l s l
s s l , s fi
s f s s l ll . M D s 2019;170:107697-708.
27 G DD, M s W, W ss K, P R. L s f f
ll s: l s, ss s s. I M R
2013;57(3):133-64.
28 L E, T s S, C s L, F A. Eff (s l l s l (SLM)
ss s s s f 316L s
s ll s s l J M P ss T l 2017;249:255-63.
29 s , S, W , L J, W P, C , l. F f s l s s f
s l s s l l s l f T 6A l 4V. A l P s A: M S
P ss 2018;124:685-98.
30 L , M, S, D W, S C. I s s
s l l s l f A l S 316L s ll s s l . M D s
2015;87:797-806.
31 L CLA, M ss S, T M, A RC, W s PJ, L PD. T ff f
f f f l s f . A M
2019;166:294-305.
32 T , K , T WQ, T J, D s s M, M l D, l. R l -
s s f α/β f l -
s l T -6A l 4V. S R 2016;6:26039-48.
33 K H, T P, L NH, T SB, C CK. G f s
ss f s l l T -6A l 4V s. V l
P s P 2016;11(3):183-91.
34 R fi HK, K NV, G H, S TL, S BE. M s s l
l . J M E P f 2013;22(12):3872-83.
35 T , K , T J, V s l G, P Q , G, l. A X l
s l T -6A l 4V. J A ll s C 2015;646:303-9.
36 R DA, M LE, M H , l. N l - s l
l f f f s l
f s l l . A M 2011;59(10):4088-99.
37 s , f s l , W H. Eff f s ll s
2018;743:258-61.
38 K S. W ll . S E 2003;23:309-48.
39 L G , G s J ff R, G s N P. E l C (111). N
L 2010;10(9):3512-6.
40 L S, C WW, C l , R ff R S. E l f
C s l l . N L 2009;9(12):4268-72.
41 W, C , W H, SQ, L. A s l l l l -f
f s f s f s. C
2020;161:479-85.
42 F AC, M JC, S V, C s C, L M, M F, l R
s f s P s R L 2006;97(18):187401-4.
43 S , G , J SH, F PC, H HQ. F l f l
- l s fi s l s l
M L 2017;200:97-100.
44 J K, H, J, C J, D . F l l f
s l f f - ll f f C -N ll CNTs.
A l S f S 2014;311:351-6.
45 R š K, M l DP, A s C, M S, S š K. X ll EMI s l
l s l s l s l
- s s f s. C s P A 2018;12:475-84.
46 S B, L , W, W. C ss l - f s
l l s f š s l l f (EMI) s l . ACS
A l M I f s 2016;8(12):8050-7.
47 L N, H , D F, H , L , G 81.8(.3(.)-306.2;(J)-278.5(.)-J7;205(S 0)-329

M 2019;34(5):489–98.

53 W B, C M, L M. R X s: l - - ffi
l f s l l s. A M
2014;26:3484–9.

54 C H, W S, J , J, X , C J, l. S ff f F₃O₄
l s fl l (l fl) s fl s
ss l s l . C s P A
2019;121:139–48.

55 W L, J, Q. T ff f MWCNTs l -
s f f -MWCNTs s s. J M S : M E l
2015;26(3):1895–9.

56 D , P GR, H P, Q F, M B , ML. Effi l
f s l fl / l s s . J. M
C 2012;22:18772–4.

57 HB, Q, WG, H , . T - l ll l
f s f l f s l . ACS A l M I f s
2011;3:918–24.

58 S A, U ll N, T l f V. T l l f
l - ll s f s l s f
M f R 2016. s:// . /10.1051/ f /2016021.

59 P s MT, J H, R ff RS, S L. T l s - s l f -
s f f l l . N L
2012;12:2959–64.

60 J K, H, H , D . P f f - ll f f C -N ll -
s s l s l f . M L
2017;122:244–7.

61 R H, L S, B S, K TW, L DS, L HJ, l. T - s l s
- s s
f . S R 2015. s:// . /10.1038/s 12710.
ss -

62 T, F SG, L , G Q, L G, R KP, l. S s l X -
l f s l l f
s s s 3D s/ ll l
l f . M S E A-S 2020. s:// . /10.1016/j
s s .2019.105670.

63 R DA, M LE, M E, H DH, M JL, M BI, l.
N l - s l f f s l
s s f s l l . A
M 2011;59(10):4088–99.

64 E s SF, L KG, S s VK, M IC. T l l s f . J T s
E l 1973;1(1):10–38.